Mon. Not. R. Astron. Soc. **000**, 000–000 (0000) Printed 28 April 2010 (MN LATEX style file v2.2)

Resolved images of self-gravitating circumstellar discs with ALMA

Peter Cossins[1], Giuseppe Lodato[2] and Leonardo Testi[3]

[1] *Department of Physics & Astronomy, University of Leicester, Leicester LE1 7RH UK*
[2] *Dipartimento di Fisica, Università Degli Studi di Milano, Via Celoria 16, 20133, Milano, Italy*
[3] *European Southern Observatory, Karl Schwarzschild str. 2, D-85748 Garching, Germany*

28 April 2010

ABSTRACT

In this paper we present simulated observations of massive self-gravitating circumstellar discs using the Atacama Large Millimetre/sub-millimetre Array (ALMA). Using a smoothed particle hydrodynamics model of a 0.2 $M_\odot$ disc orbiting a 1 $M_\odot$ protostar, with a cooling model appropriate for discs at temperatures below $\sim$ 160K and representative dust opacities, we have constructed maps of the expected emission at sub-mm wavelengths. We have then used the CASA ALMA simulator to generate simulated images and visibilities with various array configurations and observation frequencies, taking into account the expected thermal noise and atmospheric opacities. We find that at 345 GHz (870 μm) spiral structures at a resolution of a few AU should be readily detectable in approximately face-on discs out to distances of the Taurus-Auriga star-forming complex.

Key words: accretion, accretion discs – gravitation – instabilities – stars: circumstellar matter – stars: pre-main-sequence – submillimetre

1 INTRODUCTION

Circumstellar discs play an important role in the formation and evolution of both stars and planets, and as such have been the object of much study and observation in recent years. Millimetre wavelength surveys of star forming regions in Taurus (Beckwith et al., 1990; Kitamura et al., 2002; Andrews & Williams, 2005), Orion (Eisner et al., 2008) and ρ Ophiucus (Andre & Montmerle, 1994; Andrews & Williams, 2007b) have provided extensive evidence of circumstellar discs, while optical images have been provided by the Hubble Space Telescope (HST) of HH30 (Burrows et al., 1996) and the Fomalhaut system (Kalas et al., 2008). However, relatively few systems have been imaged with great enough resolution to determine the disc structure on scales of less than a few tens of *AU*.

This may be about to change however, with the Atacama Large Millimetre/sub-millimetre Array (ALMA) due to come on line in the near future. With a minimum beam diameter of approximately 5 milli-arcseconds at 900 GHz, ALMA should ideally provide resolution down to $\approx 2AU$ for discs observed in Orion, with sub-*AU* resolution for systems in Taurus-Auriga. It will therefore allow observations of disc sub-structure in unprecedented detail. The discovery of structures within discs could have important implications for our understanding of the evolution of both the discs themselves (Rice & Armitage, 2009) and the protostars they orbit.

Gaseous circumstellar discs are expected to be turbulent (Ebert, 1994; Gammie, 1996), with the internal stresses that this turbulence induces being the principal driver of angular momentum transport, and thus accretion. This turbulence will lead to substructure being present at all scales within the disc, with those on smaller scales (due to the magneto-rotational instability) remaining undetectable, while the larger scale structure induced by the gravitational instability should be resolvable with ALMA.

It is expected that protostellar discs about Class 0/Class I objects will go through a self-gravitating phase (Bertin & Lodato, 2001; Vorobyov & Basu, 2005; Hartmann, 2009) as the infall rate from the gaseous envelope is much greater than the accretion rate onto the protostar (Vorobyov & Basu, 2006). In this phase large amplitude spiral structures will form, driving accretion onto the protostar (Lin & Pringle, 1987; Laughlin & Bodenheimer, 1994; Armitage et al., 2001; Lodato & Rice, 2004, 2005) and potentially leading to the formation of companion objects. These companions may vary in size from stellar mass (Bonnell, 1994; Bonnell & Bate, 1994; Whitworth et al., 1995) to brown dwarf (BD) or planetary mass (Rice et al., 2005; Stamatellos et al., 2007; Clarke, 2009; Cossins et al., 2010). It is possible that protoplanetary discs around Classic T-Tauri (Class II) stars may also exhibit spiral patterns due to the presence of gravitational instabilities (Bertin & Lodato, 2001; Boley et al., 2006; Vorobyov & Basu, 2008; Cossins et al., 2010), and indeed there are already possible detections of spiral structures in the discs of GSS 39 in Ophiuchus (Andrews et al., 2009) and in IRAS 16293-2422B (Rodríguez et al., 2005).

At radii greater than approximately 50*AU*, planet formation through direct fragmentation of these spiral overdensities into bound objects is possible (Boss, 1997, 1998; Clarke, 2009; Rafikov, 2009; Cossins et al., 2010). While Wolf & D'Angelo (2005) have indicated that the forming giant (proto-)planets themselves may be

⋆ E-mail: peter.cossins@astro.le.ac.uk

detectable using ALMA, the observability of the large-scale spiral structure itself within protostellar and protoplanetary discs, though implied (Testi & Leurini, 2008), has remained undemonstrated. In this paper we therefore present a simple self-gravitating disc simulation, and from it we derive mock observations of disc systems at the resolutions and sensitivities that should be possible with ALMA. Hence in section 2 we detail the simulation, and in section 3 we discuss how the mock observations are generated from it, taking into account telescope effects and sensitivities. In section 4 we present the observations for various system and telescope parameters, and finally in section 5 we discuss the significance of our results.

2 NUMERICAL SIMULATION OF STRUCTURE FORMATION

Gravitational instabilities in discs have been extensively studied numerically using both grid-based Eulerian codes (Gammie, 2001; Pickett et al., 2003; Boley et al., 2006; Kratter et al., 2010) and Lagrangian particle-based methods (Rice et al., 2003; Lodato & Rice, 2004, 2005; Nayakshin et al., 2007; Alexander et al., 2008; Forgan & Rice, 2009; Cossins et al., 2009) and the reader is referred to these for further details of the dynamics of gravitationally unstable discs. The simulation we use to generate the mock observations was performed in the manner detailed in Cossins et al. (2009) using a 3D smoothed particle hydrodynamics (SPH) code, a Lagrangian hydrodynamics code capable of modelling self-gravity (see for example, Benz, 1990; Monaghan, 1992, 2005; Price & Monaghan, 2007). Our system consists of a single point mass orbited by 500,000 SPH gas particles, with the central object free to move under the gravitational influence of the disc. All particles evolve according to individual time-steps governed by the Courant condition, a force condition (Monaghan, 1992) and an integrator limit (Bate et al., 1995).

We allow the discs to cool towards gravitational instability by implementing a simple cooling law of the form

$$\frac{du_i}{dt} = -\frac{u_i}{t_{\rm cool,}i}, \tag{1}$$

where u_i and $t_{\rm cool,}i$ are the specific internal energy and cooling time associated with the i^{th} particle. We then determine the cooling time $t_{\rm cool}$ through the simple prescription that

$$\Omega t_{\rm cool} = \beta \tag{2}$$

where Ω is the angular frequency and β is a fixed parameter throughout each simulation. Although this is clearly an *ad hoc* cooling function, it can be used as a simple parameterisation in order to conduct controlled numerical experiments. In Cossins et al. (2009) we found that for a given disc mass, the spiral structures formed through the gravitational instability (as characterised by the radial and azimuthal wavenumbers of the excited modes) are *independent* of the cooling, but that the strength of the modes (characterised by the relative RMS amplitude of the surface density perturbations $\langle \delta\Sigma/\Sigma \rangle$) varies such that

$$\left\langle \frac{\delta\Sigma}{\Sigma} \right\rangle \approx \frac{1}{\sqrt{\Omega t_{\rm cool}}}. \tag{3}$$

Therefore, notwithstanding the simplicity of our cooling prescription, we may reasonably assume that the spiral structures formed in physical systems with characteristic masses corresponding to those in our simulation will have qualitatively similar structure formation, with the uncertainty lying primarily in the amplitudes of the density perturbations.

Furthermore, in Cossins et al. (2010) we characterise the behaviour of $\Omega t_{\rm cool}$ with radius, and show that for accretion rates $\sim 10^{-7}\ M_\odot\ {\rm yr}^{-1}$ (typical for Classic T Tauri objects) at radii of $20 - 50 AU$ the value of $\Omega t_{\rm cool}$ is $\sim 10^1 - 10^2$, decreasing with increasing radius. Hence although the cooling formalism given in equation 2 is very simple, it produces spiral structure in the correct modes and at approximately the correct amplitudes for the outer radii of discs, as long as we choose β in the range $\gtrsim 10$. It is therefore useful as a means of generating test cases to investigate whether such structures would actually be observable, particularly in the outer parts of discs.

2.1 Simulation Details

The simulation used to generate the mock observations described here consists of a 0.2 $M_\odot$ disc about a 1.0 $M_\odot$ mass star, extending out to approximately 25 AU. Although this is a relatively high mass ratio, it is within observed bounds (Andrews & Williams, 2005, 2007b), and is plausible for the early (Class I) stages of intermediate mass protostellar evolution, when the disc is expected to be self-gravitating (Bertin & Lodato, 2001; Vorobyov & Basu, 2005; Hartmann, 2009).

Our initial conditions consist of a disc of gas particles on circular orbits, distributed with a surface density profile $\Sigma \sim R^{-\gamma}$ with $\gamma = 1.5$, as for the Minimum Mass Solar Nebula (MMSN, Weidenschilling 1977). Note that observational constraints for γ range from $0.4 \lesssim \gamma \lesssim 1.0$ for protoplanetary discs in Ophiuchus (Andrews et al., 2009) to $0.1 \lesssim \gamma \lesssim 1.7$ in Taurus (Andrews & Williams, 2007a), so this value is within observed limits.

The disc is initially in approximate vertical hydrostatic equilibrium with a Gaussian distribution of particles where the scale height $H = c_{\rm s}/\Omega$ and $c_{\rm s}$ is the sound speed. The azimuthal velocities take into account both a pressure correction (Lodato, 2007) and the enclosed disc mass and any variation from dynamical equilibrium is washed out on the dynamical timescale. The initial temperature profile is such that $c_{\rm s}^2 \sim R^{-1/2}$, with the minimum value of the Toomre parameter $Q_{\rm min} = 2$ occurring at the outer edge of the disc. In this manner the disc is initially gravitationally stable throughout its radial range.

Note that the SPH code and the initial conditions used are exactly the same as were used in Lodato & Rice (2004, 2005) and Cossins et al. (2009, 2010), excepting the fact that here we have used a mass ratio of 0.2, and the reader is directed to these for further details. Finally, in terms of cooling, we set $\beta = 7$ and use the cooling formalism described in equation 1 above. This is approximately in the expected range, and is low enough to avoid spurious numerical heating effects due to artificial viscosity (Lodato & Rice, 2004).

2.2 Disc Evolution

Although the thermal profile of the disc initially ensures it is gravitationally stable at all radii, it is however *not* in thermal equilibrium. As the simulation evolves, the disc therefore cools towards gravitational instability, which is initiated when $Q \approx 1$, after approximately 1000 years. The disc then settles into a marginally stable, quasi-steady dynamic thermal equilibrium state, characterised by the presence of spiral density waves that propagate across the face

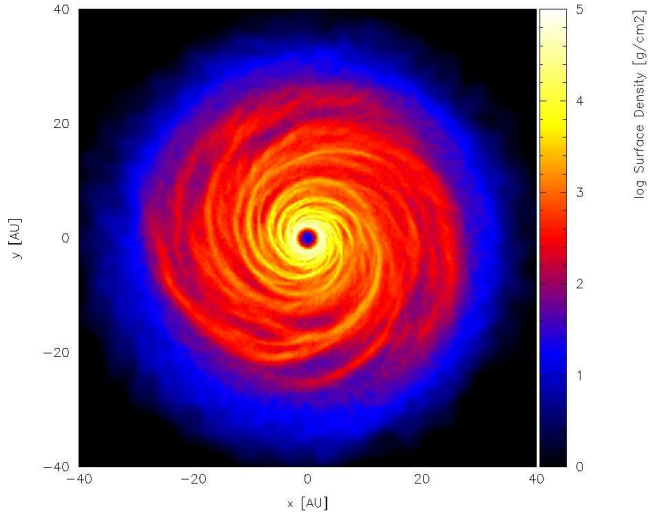

Figure 1. Simulated surface density perturbations in a 0.2 $M_\odot$ disc about a 1.0 $M_\odot$ protostar. The gravitationally induced spiral waves that impart heat to the disc are clearly visible.

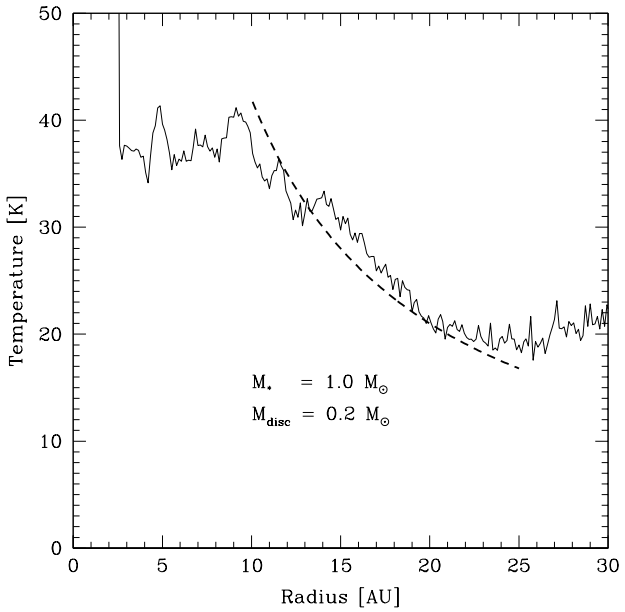

Figure 2. Azimuthally averaged temperature profile of the disc once it has settled into the dynamic thermal equilibrium state. The dashed line shows an R^{-1} profile.

of the disc, and which provide heat (through shocks) to balance the imposed cooling. These spiral waves are clearly seen in the surface density, as shown in Fig. 1. The simulation was run for approximately 10,000 years (equivalent to $\sim$ 10 cooling times at the disc outer edge), suggesting that during the self-gravitating period of protostellar evolution (expected to last a few $\times 10^5$ years during and immediately after the infall phase) circumstellar discs should indeed be able to reach this quasi-steady state. Since the surface density varies on the longer viscous timescale, the original $\Sigma \sim R^{-3/2}$ profile remains largely unchanged throughout the simulation.

Once the disc reaches the self-regulated dynamic thermal equilibrium state, the disc temperature falls to approximately 20 - 40 K, with the minimum at the disc outer edge, as shown in Fig. 2. Between roughly 10 and 25 AU the temperature falls off as R^{-1}, in reasonable agreement with observations (Andrews & Williams, 2007a). Note that the slight temperature *rise* outside of $R \approx 25$ AU is due to very low density, higher temperature gas external to the main bulk of the disc.

3 GENERATION OF MOCK OBSERVATIONS

Having run the hydrodynamic simulations, it is then necessary to use the disc parameters to create flux maps of the objects as they may appear using ALMA. Throughout the following we assume that the disc is face-on to the observer.

In order to calculate the emission we use the individual particle densities ρ_i generated from the SPH simulations, and calculate the particles' absorption coefficients $\alpha_{\nu,\mathrm{i}}$ at frequency ν using

$$\alpha_{\nu,\mathrm{i}} = \rho_\mathrm{i} \kappa_\nu, \tag{4}$$

where κ_ν is the opacity of the disc at frequency ν.

For a face-on disc the optical depth τ_ν at frequency ν is defined in the following manner

$$\tau_\nu = \int_{-\infty}^{\infty} \alpha_\nu(z)\, \mathrm{d}z, \tag{5}$$

and hence for a disc of SPH particles, we may evaluate the vertical optical depth at any point on the disc face by approximating this integral as a sum over all the relevant interacting particles. We therefore use the following approximation for the optical depth of the disc as seen by a distant observer

$$\tau_\nu \approx \sum_\mathrm{i} \rho_\mathrm{i} \kappa_\nu w_\mathrm{i} \tag{6}$$

where w_i is a weighting function related to the particle's mass, density, and the SPH smoothing kernel (see Price 2007) and where i denotes all particles along a given line of sight through the disc.

We assume that radiation from the disc is in thermal equilibrium with itself and thus that the disc emits as a black body, with the source function S_ν at frequency ν given by the Planck function,

$$S_\nu = B_\nu(T) = \frac{2h\nu^3}{c^2} \frac{1}{e^{h\nu/kT} - 1}, \tag{7}$$

where h is Planck's constant, c is the speed of light *in vacuo*, k is Boltzmann's constant and T is the temperature of the emitter. For simplicity, we assume that our discs are vertically isothermal with temperature T, (which we obtain via a vertical average from the simulations) meaning that at each point in the disc the source function is constant with height, and is given by $B_\nu(T)$. Modelling the disc in this manner, as a geometrically thin structure with no vertical temperature gradient, is obviously a very crude approximation. Nevertheless, since we are only interested in predicting the emission in the (sub-)millimetre range, this approximation is justified as the bulk of the emission will indeed come from the relatively isothermal layer located about the disc midplane.

For such a constant source function, the specific intensity (or surface brightness) I_ν at frequency ν and optical depth τ_ν is given by

$$I_\nu = B_\nu(T)\left(1 - e^{-\tau_\nu}\right). \tag{8}$$

Note that this formulation for the surface brightness is often used in reverse to infer disc properties from the (sub) millimetre surface brightness, e.g. Beckwith et al. (1990); Andrews et al. (2009). Furthermore, it is also clear that once the disc becomes optically thick

its emission is determined solely by its temperature, whereas in optically thin regions the emission is exponentially dependent on τ_ν. Optically thick structures forming in optically thin parts of the disc are therefore likely to show greater variation in intensity (and thus be more readily observable) than structure in purely optically thick regions.

3.1 Dust opacities

A critical parameter in the above calculation is the opacity of the disc κ_ν. At temperatures below $\approx 160K$ the Rosseland mean opacity becomes dominated by ices (Bell & Lin, 1994; Cossins et al., 2010), but the specific value of the opacity at a given frequency κ_ν is determined by the grain size distribution (Miyake & Nakagawa, 1993).

To determine the value of κ_ν we use the power-law model of Beckwith et al. (1990), such that

$$\kappa_\nu = \kappa_{12}\left(\frac{\nu}{\nu_{12}}\right)^\beta, \tag{9}$$

where $\nu_{12} = 10^{12}$ Hz, and where κ_{12} is the value of the opacity at this fiducial frequency. The normalisation constant κ_{12} is relatively poorly constrained, with values ranging from 0.1 cm^2 g^{-1} (Beckwith et al., 1990) to approximately 0.016 (Kramer et al., 1998; Rafikov, 2009). For protoplanetary and protostellar discs the power-law index β can be determined from the disc SED in the mm/sub-mm range, and is found to be in the region $0.3 \lesssim \beta \lesssim 1.5$ (Kitamura et al., 2002; Testi et al., 2003; Ricci et al., 2009). Note that this range is below that expected for the interstellar medium $\beta \approx 1.7 - 2$ (Finkbeiner et al., 1999; Chakrabarti & McKee, 2008; Hartmann, 2009), which is attributed to grain processing within the disc.

For our models we use a fiducial dust opacity $\kappa_{12} = 0.025$ cm^2 g^{-1}, and in accordance with Rafikov (2009) we assume throughout that $\beta = 1.0$, such that

$$\kappa_\nu = 0.025\left(\frac{\nu}{10^{12}\text{ Hz}}\right)\text{ cm}^2\text{ g}^{-1}. \tag{10}$$

3.2 The ALMA Simulator

To produce realistic simulated ALMA observations of the models we have used the ALMA simulator `simdata` in CASA[1]. The version of the simulator we used (2.4) allows us to use the latest version of the planned ALMA antenna configurations, the expected receiver noise based on technical specifications and the contribution due to the atmosphere, itself based on input values for the atmospheric temperature $T_{\rm atm}$ and the optical depth at the frequency of the simulations. In all the simulations presented here we assume $T_{\rm atm} = 265$ K, and the optical depth is computed using the ATM atmosphere models of Pardo et al. (2002). We use typical Chajnantor conditions and an amount of precipitable water vapour (pwv) as expected for dynamical scheduling of the observations. In Table 1 we therefore show the water content and opacity of the atmosphere, the expected theoretical noise and the angular and linear resolution of the simulations for discs at 50 pc and 140 pc for each frequency.

Note that we have also run simulations for the lowest (45 GHz) and highest (870 GHz) planned ALMA bands – contrary to the intermediate frequencies, these frequency bands will not be available when ALMA first comes on-line. High frequencies receivers are planned to be introduced during the early years of ALMA science operations, while the low frequency band is under discussion for the ALMA development programme.

The array configuration used varied for each frequency, as we aimed to use the configuration that offered the best compromise between surface brightness sensitivity and angular resolution. Note that at low frequencies the angular resolution is limited by the largest available array configuration. In all cases we performed aperture synthesis simulations with transit duration of 2 hrs.

[1] CASA (Common Astronomy Software Applications) is being primarily developed by ALMA and the National Radio Astronomy Observatory (NRAO) as the main off-line data reduction package for ALMA and EVLA, the Expanded Very Large Array. `http://casa.nrao.edu`

4 RESULTS

Using the disc simulation shown in Fig. 1, we investigated the emission at the various frequencies shown in Table 1. Based on the requirement that the optical depth should vary between optically thick in the spiral arms and optically thin in the inter-arm regions (to maximise the contrast in emission across these regions) we have principally considered the results at 345 GHz. Furthermore, at this frequency we expect the resolution to be roughly 1 AU at both TW Hydrae and Taurus-Auriga distances, while the telescope sensitivity should not be a limiting factor. To illustrate the effects of varying the frequency, the optical depth at 45, 345 and 870 GHz is shown in Fig. 3 for comparison. Also clear from this figure is the expected increase in optical depth with frequency due to increasing opacity.

4.1 Simulated ALMA Images

Having generated the specific intensity map by the method described in section 3, we have used them to simulate ALMA observations as described in section 3.2. In Figs 4 and 5 we therefore show the results of our simulations for discs at a distance of 50pc (TW Hya) and at 140pc (Chamaeleon, Ophiuchus, Taurus-Auriga). Note that our simulations only include the effects of thermal noise from receivers and the atmosphere, but do not take into account calibration uncertainties and residual phase noise after calibration. These effects are likely to be most important at high frequencies and long baselines, so the simulated maps at 680 and 870 GHz, especially for the 140pc case, represent observations carried out in ideal conditions and with excellent calibrations.

The simulations show that the predicted spiral structure is readily detectable at all simulated frequencies at the 50 pc distance of the TW Hya association. In the case of star-forming regions at 140pc the situation is less clear cut. At low frequencies ($\lesssim$ 100 GHz) even ALMA will probably not provide the angular resolution required to image the spiral structure clearly, whereas at the highest frequencies, as noted above, the simulations are probably over optimistic. Nevertheless, our simulations show that at 220 and 345 GHz (ALMA Bands 6 and 7), the predicted structures should be clearly detectable.

Finally, in Fig. 6 we show the predicted observability of a disc at 410pc (equivalent to the Orion Nebula Cluster distance) imaged at 345 GHz. While the non-axisymmetric nature of the disc is clear, the spiral structure *per se* is not well resolved, and thus we infer that even with ALMA such structures will not be conclusively detectable.

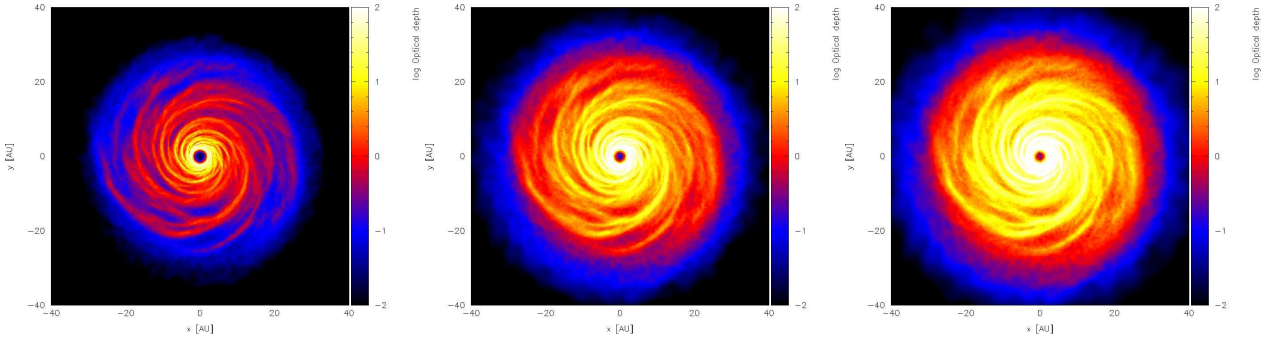

Figure 3. Comparison of the (logarithmic) optical depth across the disc face at frequencies of 45 GHz (left), 345 GHz (centre) and 870 GHz (right). The greatest contrast between optically thick and optically thin regions across the arm/inter-arm regions in the bulk of the disc is to be seen in the 345 GHz case.

Frequency	**Atmospheric Conditions**		**Expected Sensitivity**	**Resolution at 50pc**		**Resolution at 140pc**	
(GHz)	pwv (mm)	τ_0	1σ (μJy/beam)	(mas)	(AU)	(mas)	(AU)
45	2.3	0.05	3	120	6	120	16.8
100	2.3	0.03	4	50	2.5	50	7
220	2.3	0.1	10	60	3	20	2.8
345	1.2	0.2	20	40	2	25	3.5
680	0.5	0.6	60	50	2.5	35	4.9
870	0.5	0.7	100	60	3	45	6.3

Table 1. Atmospheric conditions, expected sensitivities and angular and linear resolutions as a function of frequency for the simulated observations, assuming distances of 50 pc (corresponding to the distance of the TW Hya association) and 140 pc (roughly corresponding to the Taurus-Auriga, Ophiucus and Chamaeleon star forming regions). The amount of precipitable water vapour (pwv, in mm) has been chosen according to the current ALMA dynamical scheduling expectations. Note that at the higher frequencies the varying resolutions at different distances is due to the fact that we have considered different ALMA configurations in order to obtain an optimal compromise between resolution and sensitivity. On the other hand, at low frequency, the resolution is dictated by the largest available array configuration, and thus remains constant with distance.

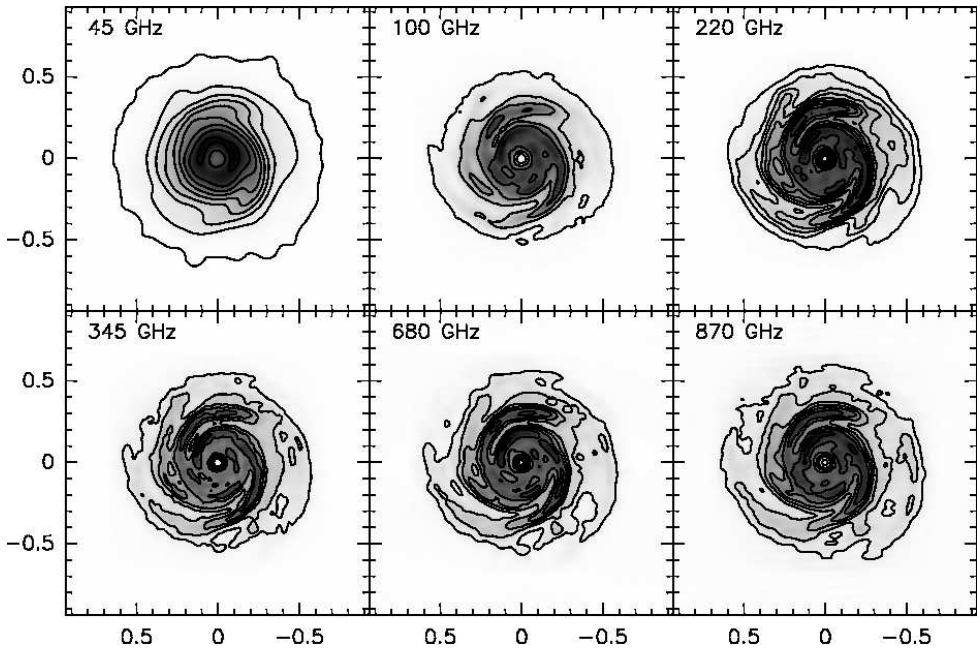

Figure 4. Simulated aperture synthesis ALMA images for a disc at 50 pc, with a transit duration of 2 hours. From left to right and top we show simulations computed for an observing frequency of 45, 100, 220 (top) and 345, 670 and 870 GHz (bottom). Axis scales are in arcseconds. Contours start at 0.01 and are spaced by 0.08 mJy/beam at 45 GHz, start at 0.08 and are spaced by 0.2 mJy/beam at 100 GHz, start at 0.5 and are spaced by 0.5 mJy/beam at 220 GHz, start at 0.8 and are spaced by 0.8 mJy/beam at 345 GHz, start at 2 and are spaced by 2 mJy/beam at 680 GHz, start at 4 and are spaced by 4 mJy/beam at 870 GHz.

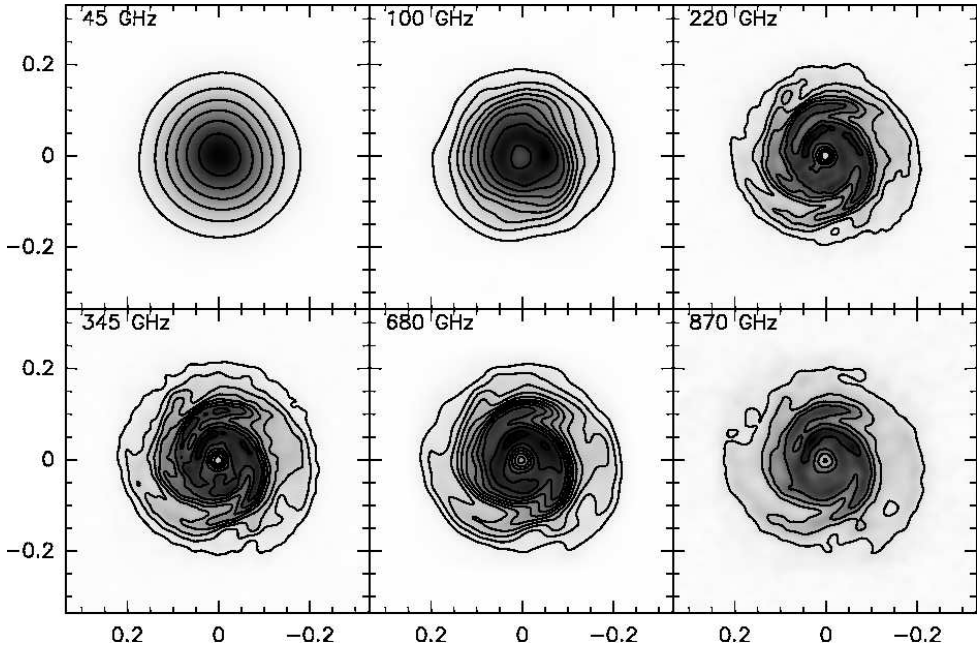

Figure 5. As for Fig. 4, but for a disc at 140 pc. Contours start at 0.08 and are spaced by 0.08 mJy/beam at 45 GHz, start at 0.08 and are spaced by 0.08 mJy/beam at 100 GHz, start at 0.1 and are spaced by 0.1 mJy/beam at 220 GHz, start at 0.2 and are spaced by 0.2 mJy/beam at 345 GHz, start at 2 and are spaced by 1 mJy/beam at 680 GHz, start at 1 and are spaced by 1 mJy/beam at 870 GHz.

5 DISCUSSION

In this paper, we have used a 3D, global SPH simulation of a massive (0.2 $M_\odot$) compact ($R_{\rm out}$ = 25 AU) self-gravitating disc about a young star (1.0 $M_\odot$) to demonstrate that the spiral modes excited by the gravitational instability should be detectable in face-on circumstellar discs using ALMA. At distances comparable to the TW Hydrae association ($\sim$ 50 pc), such spiral density waves are readily apparent with observation times of 2 hours, whereas at Taurus distances of $\sim$ 140 pc a careful choice of the observing frequency and excellent observing conditions may be required for significant detections. Our results suggest that structure in such discs in Orion ($\sim$ 400pc) will most likely not be resolvable.

In order to generate these predicted observations we have used temperature and density maps provided by numerical simulations, together with an empirical relationship for the dust opacity of circumstellar material to obtain the optical depth at each part of the disc face. In a precisely similar manner to that used to obtain disc properties from sub-mm observations (Beckwith et al., 1990) we have then been able to determine the specific intensity of the disc emission across the disc face, which has then been used as input for the ALMA simulator in CASA to produce simulated observations. We find that observation frequencies of around 345 GHz (870 μm) are ideal for this kind of observation, as we find the spiral arms to be optically thick, whereas the inter-arm regions are optically thin, maximising the contrast in emission between the regions. It should be noted however that this 'ideal' frequency range is dependent on our assumptions concerning the dust opacity, in which there is considerable scatter.

There are certain limitations to our model which should be noted however. Our stellar and disc masses are both at the upper end of the expected distributions (Andrews & Williams, 2005, 2007b; Beckwith et al., 1990), although in the early stages of star formation (Class I objects) such high disc masses are not unreasonable due to the infalling envelope. Of necessity, in order to be self-gravitating our discs are cold (20 – 40 K), which implies both a relatively low ambient temperature (not unreasonable, since giant molecular clouds tend to have temperatures of $\sim 10K$, Myers et al. 1983; Myers & Benson 1983) and for heating from the protostar to be negligible. While this latter assumption is clearly unlikely to be valid for the surface layers of the disc that are irradiated directly by the star, the disc midplane (which dominates the emission) is likely to be cold enough to justify this assumption (Andrews & Williams, 2005; Dullemond et al., 2007; D'Alessio et al., 1998). In a similar manner, this assumption of a colder inner layer allows us to ignore the effects of the magneto-rotational instability (Gammie, 1996).

Given that our disc is quite compact, and many discs are observed to extend out to much larger radii ($\sim 10^2 - 10^3$ AU, Andrews et al. 2009; Eisner et al. 2008; Andrews & Williams 2007b; Kitamura et al. 2002) the colder regions outside of $\sim$ 50 AU are if anything more likely to show evidence of gravitational instability that at the radii we simulate, and indeed any spiral structures forming at large radii will be more easily resolvable. In this sense therefore our predictions may even be conservative in terms of the maximum distance at which spiral structures may be detectable.

Likewise our cooling prescription, although simplistic, is valid for regions at large radii where the temperature is below the ice sublimation temperature, and is therefore not an unreasonable simplification. It should be noted that the ratio of the cooling time to the dynamical time $\beta = t_{\rm cool}\Omega$ determines the amplitude of the spiral perturbation and hence the contrast in the simulated images. The value $\beta = 7$ adopted in this paper is in the right range for discs at a few tens of AU. However, a larger value of β (that is, a less efficient cooling) would provide a relatively smaller contrast in the ALMA images.

Finally, note that in this paper we have considered the contribution to the sub-millimetre emission due solely by the disc. In the earliest phases of star formation, the system might show a substantial emission on larger scales, produced by the infalling envelope

feeding the disc. This larger scale contribution has been neglected in the present paper.

As noted in the Introduction there are already possible detections of spiral structures in the discs of GSS 39 in Ophiuchus (Andrews et al., 2009) and in IRAS 16293-2422B (Rodríguez et al., 2005). However the structures in GSS 39 are not robust at the 3σ level (Andrews et al., 2009), and those in IRAS 16293-2422B, whilst appearing to be genuine, may plausibly be due to interactions with a companion. Furthermore, the presence of planetary mass objects within the disc may also lead to the excitation of spiral density waves (see for instance Goldreich & Tremaine, 1980; Ogilvie & Lubow, 2002; Armitage & Rice, 2005). However in this latter case the one-armed spiral wakes are in general tightly wound (dependent on the disc thickness, Ogilvie & Lubow 2002) and would therefore be difficult to detect directly. Furthermore, analysis by Wolf & D'Angelo (2005) on the observability of embedded gas giant planets using ALMA suggests that the spirals would only be visible very close to the planet itself. Any detections of large scale spirals in isolated protostellar discs are therefore likely to be due principally to the action of the gravitational instability.

Confirmed, unambiguous observations of gravitationally induced spiral structures within protostellar discs would be valuable for a number of reasons. As the gravitational instability is expected to operate during the early phases of star formation, processing the infalling envelope and allowing rapid accretion onto the protostar, such detections would validate this mechanism for growing the masses of protostars. More controversially, it may enable models of brown dwarf/low mass stellar companion formation through disc fragmentation (Bate et al., 2002; Stamatellos et al., 2007; Stamatellos & Whitworth, 2009; Clarke, 2009) to be validated, as the presence (or otherwise) and amplitudes of spiral arms would allow constraints to be placed on the numbers of such companions that may be expected.

In a similar vein, detections of spiral features may enable us to determine the dominant mode of planet formation at various radii, about which there is some debate. While the standard core-accretion model is favoured at low radii (Boley, 2009; Klahr, 2008; Bodenheimer et al., 2000; Lissauer, 1993), direct fragmentation of gravitationally induced spirals remains a candidate mechanism at radii above ~ 50 AU (Boss, 1997; Boley et al., 2006; Rafikov, 2009; Cossins et al., 2010). As the presence of a peak in the 1.3 cm emission around HL Tau has been put forward as a promising candidate for a planetary mass companion formed through gravitational instability, detections of the spiral wave progenitors of such companions would provide significant backing for this mechanism. Moreover, the presence of large amplitude spiral density perturbations may be important for the formation and growth of planetesimals, both due to the concentration of the dust fraction within the arms (Rice et al., 2004, 2006; Clarke & Lodato, 2009) and further due to the possible scattering of planetesimals by the spiral potential (Britsch et al., 2008). In either case, observations of the spiral arms themselves would place constraints on, and therefore allow us to discriminate between, the two planet formation modes at large radii.

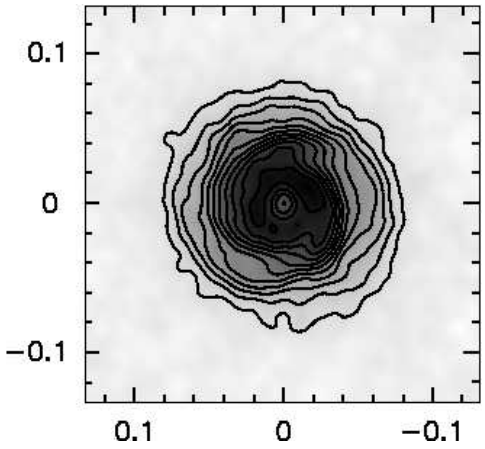

Figure 6. Simulated 345 GHz aperture synthesis image of a disc at 410 pc, with a transit duration of 2 hours. Contours start at and are spaced by 60 mJy/beam. Clear asymmetries are present, but the underlying spiral structure is not well resolved.

ACKNOWLEDGEMENTS

We acknowledge the use of SPLASH (Price, 2007) for the rendering of all surface density and optical depth plots. PJC would further like to thank Mark Wilkinson for helpful discussions concerning observational techniques.

REFERENCES

Alexander R. D., Armitage P. J., Cuadra J., 2008, MNRAS, 389, 1655
Andre P., Montmerle T., 1994, ApJ, 420, 837
Andrews S. M., Williams J. P., 2005, ApJ, 631, 1134
Andrews S. M., Williams J. P., 2007a, ApJ, 671, 1800
Andrews S. M., Williams J. P., 2007b, ApJ, 659, 705
Andrews S. M., Wilner D. J., Hughes A. M., Qi C., Dullemond C. P., 2009, ApJ, 700, 1502
Armitage P. J., Livio M., Pringle J. E., 2001, MNRAS, 324, 705
Armitage P. J., Rice W. K. M., 2005, arXiv:astro-ph/0507492
Bate M. R., Bonnell I. A., Bromm V., 2002, MNRAS, 332, L65
Bate M. R., Bonnell I. A., Price N. M., 1995, MNRAS, 277, 362
Beckwith S. V. W., Sargent A. I., Chini R. S., Guesten R., 1990, AJ, 99, 924
Bell K. R., Lin D. N. C., 1994, ApJ, 427, 987
Benz W., 1990, in Buchler J. R., ed., Numerical Modelling of Nonlinear Stellar Pulsations Problems and Prospects p. 269
Bertin G., Lodato G., 2001, A&A, 370, 342
Bodenheimer P., Hubickyj O., Lissauer J. J., 2000, Icarus, 143, 2
Boley A. C., 2009, ApJL, 695, L53
Boley A. C., Mejía A. C., Durisen R. H., Cai K., Pickett M. K., D'Alessio P., 2006, ApJ, 651, 517
Bonnell I. A., 1994, MNRAS, 269, 837
Bonnell I. A., Bate M. R., 1994, MNRAS, 269, L45
Boss A. P., 1997, Science, 276, 1836
Boss A. P., 1998, ApJ, 503, 923
Britsch M., Clarke C. J., Lodato G., 2008, MNRAS, 385, 1067
Burrows C. J., Stapelfeldt K. R., Watson A. M., Krist J. E., Ballester G. E., Clarke J. T., Crisp D., Gallagher III J. S., Griffiths R. E., Hester J. J., Hoessel J. G., Holtzman J. A., Mould J. R., Scowen P. A., Trauger J. T., Westphal J. A., 1996, ApJ, 473, 437
Chakrabarti S., McKee C. F., 2008, ApJ, 683, 693
Clarke C. J., 2009, MNRAS, 396, 1066
Clarke C. J., Lodato G., 2009, MNRAS, 398, L6
Cossins P., Lodato G., Clarke C., 2010, MNRAS, 401, 2587
Cossins P., Lodato G., Clarke C. J., 2009, MNRAS, 393, 1157
D'Alessio P., Canto J., Calvet N., Lizano S., 1998, ApJ, 500, 411
Dullemond C. P., Hollenbach D., Kamp I., D'Alessio P., 2007, in Reipurth B., Jewitt D., Keil K., eds, Protostars and Planets V Models of the Structure and Evolution of Protoplanetary Disks. pp 555–572
Ebert R., 1994, A&A, 286, 997
Eisner J. A., Plambeck R. L., Carpenter J. M., Corder S. A., Qi C., Wilner D., 2008, ApJ, 683, 304
Finkbeiner D. P., Davis M., Schlegel D. J., 1999, ApJ, 524, 867
Forgan D., Rice K., 2009, MNRAS, 400, 2022

Gammie C. F., 1996, ApJ, 457, 355
Gammie C. F., 2001, ApJ, 553, 174
Goldreich P., Tremaine S., 1980, ApJ, 241, 425
Hartmann L., 2009, Accretion Processes in Star Formation: Second Edition. Cambridge University Press
Kalas P., Graham J. R., Chiang E., Fitzgerald M. P., Clampin M., Kite E. S., Stapelfeldt K., Marois C., Krist J., 2008, Science, 322, 1345
Kitamura Y., Momose M., Yokogawa S., Kawabe R., Tamura M., Ida S., 2002, ApJ, 581, 357
Klahr H., 2008, New Astronomy Review, 52, 78
Kramer C., Alves J., Lada C., Lada E., Sievers A., Ungerechts H., Walmsley M., 1998, A&A, 329, L33
Kratter K. M., Matzner C. D., Krumholz M. R., Klein R. I., 2010, ApJ, 708, 1585
Laughlin G., Bodenheimer P., 1994, ApJ, 436, 335
Lin D. N. C., Pringle J. E., 1987, MNRAS, 225, 607
Lissauer J. J., 1993, ARA&A, 31, 129
Lodato G., 2007, Nuovo Cimento Rivista Serie, 30, 293
Lodato G., Rice W. K. M., 2004, MNRAS, 351, 630
Lodato G., Rice W. K. M., 2005, MNRAS, 358, 1489
Miyake K., Nakagawa Y., 1993, Icarus, 106, 20
Monaghan J. J., 1992, ARA&A, 30, 543
Monaghan J. J., 2005, Reports on Progress in Physics, 68, 1703
Myers P. C., Benson P. J., 1983, ApJ, 266, 309
Myers P. C., Linke R. A., Benson P. J., 1983, ApJ, 264, 517
Nayakshin S., Cuadra J., Springel V., 2007, MNRAS, 379, 21
Ogilvie G. I., Lubow S. H., 2002, MNRAS, 330, 950
Pardo J., Cernicharo J., Serabyn E., 2002, in J. Vernin, Z. Benkhaldoun, & C. Muñoz-Tuñón ed., Astronomical Site Evaluation in the Visible and Radio Range Vol. 266 of Astronomical Society of the Pacific Conference Series, Modeling the atmospheric longwave spectrum: State of the art in the horizon of ALMA. p. 188
Pickett B. K., Mejía A. C., Durisen R. H., Cassen P. M., Berry D. K., Link R. P., 2003, ApJ, 590, 1060
Price D. J., 2007, Publications of the Astronomical Society of Australia, 24, 159
Price D. J., Monaghan J. J., 2007, MNRAS, 374, 1347
Rafikov R. R., 2009, ApJ, 704, 281
Ricci L., Testi L., Natta A., Neri R., Cabrit S., Herczeg G. J., 2009, arXiv:0912.3356
Rice W. K. M., Armitage P. J., 2009, MNRAS, 396, 2228
Rice W. K. M., Armitage P. J., Bate M. R., Bonnell I. A., 2003, MNRAS, 339, 1025
Rice W. K. M., Lodato G., Armitage P. J., 2005, MNRAS, 364, L56
Rice W. K. M., Lodato G., Pringle J. E., Armitage P. J., Bonnell I. A., 2004, MNRAS, 355, 543
Rice W. K. M., Lodato G., Pringle J. E., Armitage P. J., Bonnell I. A., 2006, MNRAS, 372, L9
Rodríguez L. F., Loinard L., D'Alessio P., Wilner D. J., Ho P. T. P., 2005, ApJ, 621, L133
Stamatellos D., Hubber D. A., Whitworth A. P., 2007, MNRAS, 382, L30
Stamatellos D., Whitworth A. P., 2009, MNRAS, 392, 413
Testi L., Leurini S., 2008, New Astronomy Review, 52, 105
Testi L., Natta A., Shepherd D. S., Wilner D. J., 2003, A&A, 403, 323
Vorobyov E. I., Basu S., 2005, ApJL, 633, L137
Vorobyov E. I., Basu S., 2006, ApJ, 650, 956
Vorobyov E. I., Basu S., 2008, ApJ, 676, L139
Weidenschilling S. J., 1977, Ap&SS, 51, 153
Whitworth A. P., Chapman S. J., Bhattal A. S., Disney M. J., Pongracic H., Turner J. A., 1995, MNRAS, 277, 727
Wolf S., D'Angelo G., 2005, ApJ, 619, 1114